Water Research 214 (2022) 118155

Contents lists available at ScienceDirect

Water Research

journal homepage: www.elsevier.com/locate/watres

Viscous and filamentous bulking in activated sludge: Rheological and hydrodynamic modelling based on experimental data

V. Bakos [a,b,*], B. Gyarmati [c], P. Csizmadia [d], S. Till [d], L. Vachoud [e], P. Nagy Göde [f], G.M. Tardy [a], A. Szilágyi [c], A. Jobbágy [a], C. Wisniewski [e]

[a] Department of Applied Biotechnology and Food Science, Faculty of Chemical Technology and Biotechnology, Budapest University of Technology and Economics, Műegyetem rkp. 3., H-1111 Budapest, Hungary
[b] Department of Chemical Engineering, University of Bath, Claverton Down, Bath, BA2 7AY, UK
[c] Department of Physical Chemistry and Materials Science, Faculty of Chemical Technology and Biotechnology, Budapest University of Technology and Economics, Műegyetem rkp. 3., H-1111 Budapest, Hungary
[d] Department of Hydrodynamic Systems, Faculty of Mechanical Engineering, Budapest University of Technology and Economics, Műegyetem rkp. 3., H-1111 Budapest, Hungary
[e] Qualisud, Université de Montpellier, CIRAD, Institut Agro, Avignon Université, Université de La Réunion, Montpellier, France
[f] DMRV Co. Ltd., Kodály Zoltán út 3., H-2600 Vác, Hungary

ARTICLE INFO

Keywords:
Activated sludge
Filamentous bulking
Viscous bulking
Non-Newtonian flow
Computational fluid dynamics
Hydrodynamics
2010 MSC:
00-01
99-00

ABSTRACT

Although achieving good activated sludge settleability is a key requirement for meeting effluent quality criteria, wastewater treatment plants often face undesired floc structure changes. Filamentous bulking has widely been studied, however, viscous sludge formation much less investigated so far. Our main goal was to find relationship between sludge floc structure and related rheological properties, moreover, to estimate pressure loss in pipe networks through hydrodynamic modelling of the non-Newtonian flows in case of well settling (ideal-like), viscous and filamentous sludge. Severe viscous and filamentous kinds of bulking were generated separately in continuous-flow lab-scale systems initially seeded with the same reference (ideal-like) biomass and the entire evolution of viscous and filamentous bulking was monitored. The results suggested correlation between the rheological properties and the floc structure transformations, and showed the most appropriate fit for the Herschel-Bulkley model (vs. Power-law and Bingham). Validated computational fluid dynamics studies estimated the pipe pressure loss in a wide Reynolds number range for the initial well settling (reference) and the final viscous and filamentous sludge as well. A practical standard modelling protocol was developed for improving energy efficiency of sludge pumping in different floc structure scenarios.

1. Introduction

Activated sludge (AS) system is the most commonly applied treatment technology in municipal wastewater treatment worldwide. Unfavorable influent wastewater quality (Tardy et al., 2012), inappropriate bioreactor arrangement and/or operational conditions may lead to filamentous (Wanner and Jobbágy, 2014) or viscous bulking (Jobbágy et al., 2017; Kiss et al., 2011) resulting in poor sludge settling. While a number of domestic wastewater treatment plants (WWTPs) face the overgrowth of filaments (Bakos et al., 2019), especially, in the winter period, viscous bulking is the typical problem of WWTPs receiving nutrient (N and P) deficient wastewater of the food industry (e.g. winery or beverage industry wastewater, etc.) (Jobbágy et al., 2002; Wanner and Jobbágy, 2014).

Both of the above mentioned undesired changes in floc structure might seriously affect the flow properties of the sludge, thus monitoring rheological characteristics is of utmost importance. Structure and shape of sludge flocs highly depend on shear stress resulting in non-Newtonian flow behavior. The change in particle size, shape and volume fraction of solids, as well as the nature of the liquid phase may largely affect the viscosity of the suspension. Consequently, both filamentous and viscous bulking may cause drastic changes in rheological properties. The main influencing factors of AS rheological properties are the total suspended solids (TSS) or mixed liquor suspended solids (MLSS) concentration (Baudez, 2008; Seyssiecq et al., 2008), temperature (Baroutian et al., 2013) including the effect of thermal hydrolysis (Farno et al., 2016; Hii et al., 2019; 2017), pH and sludge age (Hong et al., 2016; 2018;

* Corresponding author.
E-mail address: bakos.vince@vbk.bme.hu (V. Bakos).

https://doi.org/10.1016/j.watres.2022.118155
Received 6 July 2021; Received in revised form 4 January 2022; Accepted 31 January 2022
Available online 3 February 2022

Nomenclature

$\dot{\gamma}$	shear rate (s^{-1})
ζ	loss coefficient
μ	dynamic viscosity or consistency index, $(Pas), (Pa{\cdot}s^n)$
ρ	density (kg/m^3)
τ	shear stress (Pa)
τ_0	yield stress (Pa)
AS	activated sludge
B	Bingham
COD	chemical oxygen demand (mg/l)
DO	dissolved oxygen (mg/l)
DSVI	diluted sludge volume index (cm^3/g)
EPS	extracellular polymeric substances
HB	Herschel-Bulkley
MLSS	mixed liquor suspended solids (g/l)
PL	Power-law (Ostwald model)
S	substrate
SVI	sludge volume index (cm^3/g)
TSS	total suspended solids (g/l)
WWTP	wastewater treatment plant
D	internal diameter of the pipe (m)
f	friction factor
k	consistency index $(Pa{\cdot}s^n)$
L	length of the straight pipe (m)
m	local gradient of the shear stress-shear rate in a log-log diagram
n	flow behaviour index
Δp_e	pressure drop caused by the elbow (Pa)
Q	flow rate (m^3/s)
r	radius of curvature (m)
R	Pearson correlation coefficient
Re	Reynolds-number
Re_{mod}	modified Reynolds-number
RSP	Spearman correlation coefficient
$\bar{v}$	mean velocity (m/s)
y^+	dimensionless wall distance

Seyssiecq et al., 2003), while the source of the sample (i.e. primary, mixed, excess biological or digested sludge), the nature of the compounds present in solid and liquid compartments of AS (Vachoud et al., 2019), as well as the presence and type of conditioning agents may also have an effect (Hong et al., 2018; Wang et al., 2017). Since rheological properties of AS strongly affect its biogas production capacity and dewatering ability, numerous studies aim to understand the hydraulics of anaerobic digesters (Eshtiaghi et al., 2012) and the compressibility in the solid-liquid separation process as well (Stickland, 2015).

The relationship between AS floc structure changes and rheological properties is still not fully understood. Wágner et al. (2015) investigated rheological and settling parameters for quantifying and modelling filamentous bulking and reported that the impact of different filamentous species (i.e. *Microthrix parvicella* and *Chloroflexi*) on settling velocities can be remarkable. Additionally, they found that abundance of *Microthrix parvicella* can associate with hindered settling velocity and yield stress at high TSS concentrations of $8-15\ gMLSS/l$. However, to our knowledge, the entire evolution processes of viscous and filamentous bulking have not been characterized by rheological measurements so far.

In this study our main goal was to find relationship between floc structure changes (i.e. extracellular polymeric substances (EPS) content and filamentous bacteria abundance) and rheological properties (i.e. dynamic viscosity, consistency index, flow behavior index) during the evolution of viscous and filamentous bulking. The most relevant rheological characteristics were identified; not only dynamic viscosity, but also consistency and flow behavior index were estimated. To our knowledge, this work implemented for the first time the simultaneous and integrated full biotechnological and rheological tracking of viscous and filamentous bulking. Changes in flow behavior may affect oxygen mass transfer, as well as aeration and pumping-related energy consumption and costs (Eshtiaghi et al., 2013; Zhang et al., 2012). Thus, the hydrodynamic behavior was calculated by computational fluid dynamics (CFD) for estimating pressure losses in pipe networks, as well as friction losses and loss coefficients of a defined pipe/elbow configuration in case of a well settling reference (ideal-like) and for viscous and filamentous floc structures using the most frequently applied non-Newtonian models (Baroutian et al., 2013; Baudez et al., 2013). Although numerous studies are available to describe the non-Newtonian flow field inside pipes and elbows (Cabral et al., 2011; Csizmadia and Hos, 2014; Csizmadia and Till, 2018; Khandelwal et al., 2015; Pinho and Whitelaw, 1990), additional originality of the paper resides in data calculated on the basis of carefully measured fluid properties and for a wide range of Reynolds numbers.

2. Materials and methods

2.1. Continuous-flow lab-scale experiments

Continuous-flow comparative lab-scale experiment was carried out by applying two identical technological layouts during 30 days. While N and P (nutrient) deficient feed was used for *Viscous system*, simultaneously, another continuous-flow lab-scale system was operated with the same bioreactor arrangement under low S - low DO (low Substrate and low Dissolved Oxygen concentration) conditions (*Filamentous system*) for encouraging the growth of filaments (Bakos et al., 2019; Jobbágy et al., 2000; 2019). The technological set-ups consisted of one aerated basin and a secondary clarifier each (Fig. 1). Both systems were fed by synthetic wastewater freshly prepared every day and stored at $7-9^{\circ}C$ during the experiment.

Nutrient deficient feed of *Viscous system* modelled winery

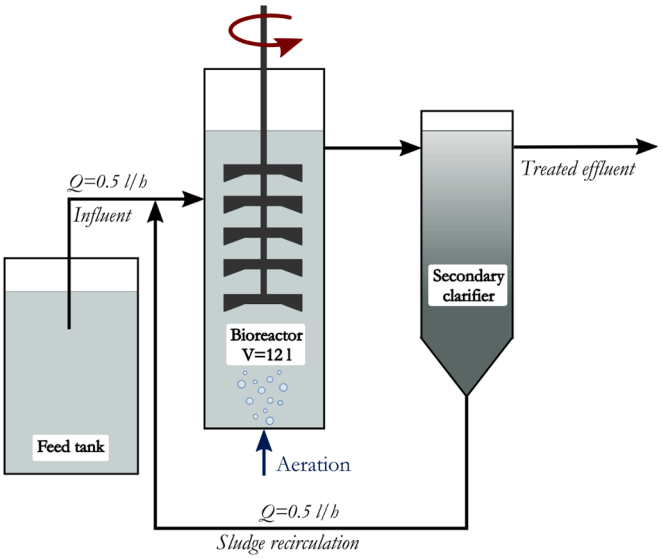

Fig. 1. Physical layout and operational parameters of the experimental systems.

wastewater, thus serious N and P deficiency was ensured (Bakos et al., 2016; Jenkins et al., 2004; Jobbágy et al., 2017) according to the components and concentrations presented in Table 1. *Filamentous system* was fed by synthetic wastewater providing marginal influent rbCOD (readily biodegradable Chemical Oxygen Demand) and nutrient availability in order to achieve low S conditions in the bioreactor (Bakos et al., 2016; Jobbágy et al., 2019; Table 1). While intensive aeration was set for the bioreactor of *Viscous system*, poor oxygen input was applied for *Filamentous system* in order to keep low DO conditions. Table 2 lists the measurements carried out during the 30-day long experiment. A hydraulic retention time of approx. 12 hours and an MLSS concentration of 3.5 g/l were maintained in the bioreactor which is in the typical biomass concentration range commonly applied in conventional AS bioreactors and also widely used for sludge settleability tests.

Sample preparation for the measurement of dissolved components (centrifuged-filtered COD, NH_4N, NO_3N, PO_4P) was carried out by Hermle Z323 centrifuge at 12,000 *rpm* for 10 *min* and supernatant was filtered by filter membrane with a pore size of 0.45μm. COD (Chemical Oxygen Demand), ammonium, nitrate, phosphate, mixed liquor suspended solids (MLSS) concentrations, sludge volume index (SVI) and diluted sludge volume index (DSVI) were measured according to the international standards (APHA, 1999). For DSVI measurements mixed liquor samples were diluted two-fold with the use of treated effluent wastewater of each system. AS floc structure changes were monitored by qualitative microscopic observation methods (S-test, Gram, Neisser, PHA and India ink staining; Jenkins et al. (2004)) by an Olympus CX41 microscope. Quantitative determination of filamentous bacteria abundance was provided by optical software through image analysis (Nagy Göde, 2010), basically similar to the method of Motta et al. (2001). 100μl native homogenized AS sample was spread smoothly on a microscope glass slide and dried out at room temperature. 500 pictures were taken for each dried sample in magn. 400x by an automatic microscope (Euromex, iScope) specifically modified and equipped for the measurement method. The optical software transformed the pictures to the size of 640x480 pixels and scanned every box of 40x40 pixels according to a pre-determined scanning plan. Optical investigations and evaluation were carried out by the box-counting method. According to the evaluated box-count values, each box of 40x40 pixels was classified as follows: (i) fragmented and diffuse flocs; (ii) very weak and filamentous; (iii) weak flocs; (iv) poorly compact flocs and (v) firm and compact flocs. The high number of images (500/*sample*) taken automatically could minimize the measurement uncertainty (< 1%). Results were expressed in covered area (pixel) % of the microscopic image. Total as well as intra- and extracellular carbohydrate concentrations of the AS were determined according to the procedure developed by Jobbágy et al. (2002).

The capillary suction time (CST) was measured for investigating sludge dewatering ability for the different biomass floc structure scenarios by CST equipment of Triton Electronics Ltd. (Dunmow, UK).

Table 1
Components and composition of synthetic influents.

Feed components and concentrations			
Components	Dimension	Viscous system	Filamentous system
Sucrose	mg/l	600	0
Na-acetate*3H_2O	mg/l	1967	287
Semi-sweet white wine	mg/l	6.67	0
Peptone	mg/l	0	113
K_2HPO_4	mg/l	15	28
$MgCl_2$	mg/l	16.7	16.7
$CaCl_2$	mg/l	36	36
Measured influent composition			
Components	**Dimension**	**Viscous system** min. - max.	**Filamentous system** min. - max.
COD	mg/l	2084 - 2428	251 - 296
BOD_5	mg/l	1771 - 1967	201 - 254
TN	mg/l	1.1 - 8.2	11.7 - 18.2
NH_4N	mg/l	0.1 - 0.6	4.2 - 11.6
PO_4P	mg/l	2.0 - 2.9	2.1 - 3.3

Table 2
Analytical measurements and their frequency applied for experimental follow-up (special abbreviations: INF: Influent; BR: Bioreactor; EFF: Effluent; 2/w: 2 times/week).

Component/property measured	Sampling point	Frequency
Temperature	INF, BR	Daily
pH	INF, BR	Daily
DO concentration	BR	Daily
Total COD concentration	INF, EFF	Daily
Centrifuged, filtered COD concentration	BR, EFF	Daily
MLSS concentration	BR	Daily
Ammonia concentration	INF, BR, EFF	3/w
Phosphate concentration	INF, BR, EFF	3/w
Nitrate concentration	BR, EFF	3/w
SVI and DSVI	BR	Daily
CST	BR	2/w
Microscopic observations and staining	BR	Daily
Total, intra- and extracellular carbohydrate content	BR	1–2/w
Rheological measurements	BR	2–3/w

2.2. Assessing the fit of rheological models

The flow behaviour of the sludge was characterized by applying an Anton Paar Physica MCR 301 rheometer equipped by double gap setup in rotation mode. The internal and external gaps of double gap geometry were e_1=0.989 mm and e_2=1.136 mm, respectively, applying gap sizes min. 10 times higher than the activated sludge floc diameters measured (80–100 μm) for safely avoiding blockage of the flow during the rheological measurements (Mori et al., 2006; Ratkovich et al., 2013; Vachoud et al., 2019). MLSS concentration of the samples taken from the bioreactor was set carefully to 3.5g/l preceding rheological measurements by slight decantation or dilution with treated effluent. The viscosity of AS was measured for a shear rate range of $1-100s^{-1}$ with three repetitions for each sample.

Based on the literature recommendation (Baroutian et al., 2013; Baudez et al., 2013; Ratkovich et al., 2013), (1) the Power-law (PL), (2) the Bingham (B) and (3) the Herschel-Bulkley (HB) rheological models were fit to the measured data, i.e.

$$\tau = k\dot{\gamma}^n, \tag{1}$$

$$\tau = \tau_{0,B} + \mu_B\dot{\gamma}, \tag{2}$$

$$\tau = \tau_{0,HB} + \mu_{HB}\dot{\gamma}^{n_{HB}}. \tag{3}$$

where τ denotes the shear stress, $\dot{\gamma}$ is the shear rate, k is the flow consistency index in case of PL model, $\tau_{0,B}$ and $\tau_{0,HB}$ are the yield stresses, μ_B and μ_{HB} are the dynamic viscosities of B and HB fluids, respectively, in addition n and n_{HB} are the flow behavior indices of PL and HB liquids.

All the three previously specified models were fit to the measured three rheograms (i.e. 3 repetitions of shear stress - shear rate curves for each sample on each sampling day) both for *Viscous system* and *Filamentous system*. These model fittings were performed through linear and nonlinear (trust region reflective) least squares algorithms in OriginPro 8.5 software.

2.3. Definition of losses and reynolds numbers

To characterize the hydrodynamic behavior of the AS suspension, dimensionless parameters were introduced according to Eq. (4) and (5). The friction factor (f) was determined from the total pressure drop of a fully developed flow in a straight pipe section with a length of L before the fitting, i.e.

$$f = \frac{\Delta p}{\frac{L}{D}\frac{\rho}{2}\overline{v}^2}, \tag{4}$$

where Δp is the total pressure drop in the pipe section, ρ is the fluid density (supposed to be equal to water density), L is the length of the section, D is the inner diameter of the pipe and $\overline{v}$ is the average flow velocity. In case of laminar flow of B plastic fluids the friction factor was determined by the Buckingham-Reiner equation (see e.g. Swamee and Aggarwal (2011a)). For HB laminar flow an explicit equation for friction was applied according to Swamee and Aggarwal (2011b) which is Reynolds number and Hedström-number dependent. The loss coefficient of an elbow ζ was defined as the non-dimensional difference in total pressure caused by the fitting (Csizmadia and Hos, 2014), i.e.

$$\zeta = \frac{\Delta p_e}{\frac{\rho}{2}\overline{v}^2}, \tag{5}$$

where Δp_e denotes the total pressure drop which was calculated between the beginning of the elbow and the end of a subsequent plane section after this fitting in a distance of $9D$. The loss caused by the wall friction in a straight pipe of the same length was subtracted but the forward disturbance of the fitting was taken into consideration according to the method developed and verified by Csizmadia and Till (2018).

In principle, the Reynolds number, as being the ratio of inertial forces to viscous forces, is given as $Re = vD\rho/\mu$ for Newtonian fluids. For laminar and fully developed flow for cylindrical pipes, the Darcy friction factor can be defined as $f_D = 64/Re$ which is generally valid for fluids regardless to their rheological characteristics (Metzner and Reed, 1955). Madlener et al. (2009) introduced an extended version of the modified Reynolds number (Re_{mod}) for PL, B or HB type of fluids, defined in Eqs. (6) and (7), i.e.

$$Re_{mod} = \frac{\overline{v}^{2-n} D^n \rho}{\frac{\tau_0}{8}\left(\frac{D}{\overline{v}}\right)^n 8^{n-1}\mu\left(\frac{3m+1}{4m}\right)^n}, \tag{6}$$

with

$$m = \frac{n\mu\left(\frac{8\overline{v}}{D}\right)^n}{\tau_0 + \mu\left(\frac{8\overline{v}}{D}\right)^n}, \tag{7}$$

where n is the flow behaviour index, τ_0 is the yield stress and μ is the dynamic viscosity; furthermore m is the local gradient (depending on $\overline{v}$) of the shear stress - shear rate curve in a log-log diagram (Madlener et al., 2009). The necessity of modification in Reynolds numbers, as well as the consequent favorable effects on further data applicability and adaptability were demonstrated earlier by Csizmadia and Till (2018). Under laminar flow conditions the Darcy friction factor can be calculated from the modified Reynolds number in case of non-Newtonian fluids, i.e. $f_D = 64/Re_{mod}$ (Csizmadia and Till, 2018; Madlener et al., 2009; Monteiro and Bansal, 2010). Moreover, the use of Re_{mod} in the turbulent region is also valid (Csizmadia and Till, 2018).

2.4. Computational fluid dynamics simulation set-up (geometry, meshing and numerics)

A typical geometry from the most commonly used size range in industrial applications was selected for the numerical simulations, i.e. a pipe section with the diameter of $d = 0.1m$ and an elbow with the radius of curvature of $r/D = 1$ (Liu and Duan, 2009; Rötsch, 1999). According to former CFD results and own validated laboratory measurements of Csizmadia and Hos (2014) and Csizmadia and Till (2018), the fully structured 3D numerical O-grid type mesh (generated in ICEM CFD; Fig. 2) included 1.2 million cells. In the boundary layer near the wall, the resolution of the cells was properly configured. Following the

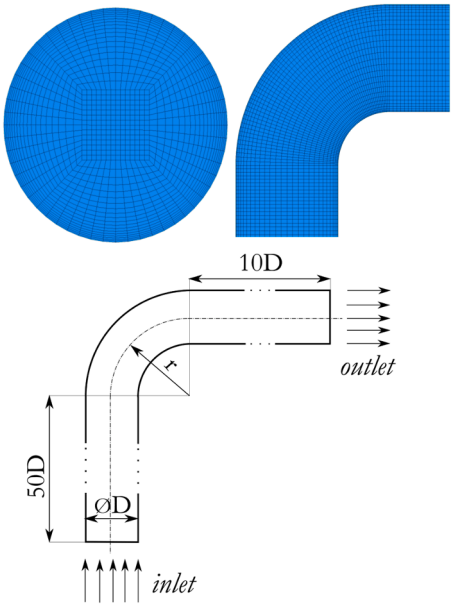

Fig. 2. Details of the numerical resolution and sketch of elbow geometry with the relative radius of curvature of $r/D = 1$ and the inner diameter of $D = 0.1m$.

calculations the y^+ dimensionless wall distance values have been verified and apart from the inlet boundary, it did not exceed the value of 1, supporting the appropriateness of the CFD model (ANSYS, 2011).

At the inlet the fully developed turbulent velocity profile for Newtonian fluids, at the outlet the average static pressure were prescribed as boundary conditions (Csizmadia and Till, 2018). The pipe was modelled as a no slip, hydraulically smooth wall. Steady state computations were performed with the commercial ANSYS-CFX software (ANSYS, 2011) by solving the Reynolds-averaged Navier-Stokes, the continuity and the transport equations associated with the actual turbulence model (Filali et al., 2013; Singh et al., 2010; White, 1991) and high-resolution spatial scheme was used for all equations. The SST (shear stress transport) turbulence model was used, which was tested previously for non-Newtonian flows (Csizmadia and Hos, 2014; Csizmadia and Till, 2018; Kfuri et al., 2011). Additional straight pipes with a length of $50D$ on the upstream and another one with a length of $10D$ on the downstream side were applied for allowing proper boundary conditions (see Fig. 2). The length set for the upstream section has been proved to be appropriate in earlier studies (Csizmadia and Till, 2018). Convergence was judged by monitoring the total pressure drop between the inlet and outlet boundaries.

The CFD calculations were carried out through all the three investigated rheological models (i.e. PL, B and HB) on the basis of the rheological data measured during the experiment. The rheological parameters, calculated by model fitting for further application in CFD study, are listed in Table 3 (in chapter 3.2.). In order to compare the hydrodynamic behavior of the different sludge floc structures, three specific states were chosen for the CFD simulations by applying rheological properties of AS taken from the (i) seeding material of the lab-scale systems on the starting day: "Reference (well settling) sludge (Start)"; (ii) *Viscous system*: "Viscous sludge (End)" and (iii) *Filamentous system*: "Filamentous sludge (End)" at the end of the experiment.

3. Results and discussion

3.1. Biotechnological implementation and biochemical monitoring of activated sludge floc structure transformations

Lab-scale experiments were first evaluated from biotechnological aspects. The bioreactor temperature varied between $17.0 - 21.5^{\circ}C$ ac-

cording to laboratory room temperature. DO concentration was as high as 6 mg/l at the start of the experiment in the intensively aerated bioreactor of *Viscous system* but it decreased to $4.0 - 4.5$ mg/l after one week of operation. Although air diffusers were regularly cleaned, intensive EPS and biofilm formation led to DO levels of $0.6 - 2.8$ mg/l in the last two weeks of the experiment. Bioreactor of *Filamentous system* was intentionally underaerated in order to ensure low DO environment. Accordingly, the DO level varied between $0.05 - 0.3$ mg/l during the whole experiment.

As expected from the operating conditions, a massive overproduction of EPS was observed in *Viscous system* (without increasing filament abundance) while serious filamentous bulking was achieved in *Filamentous system* (without excessive EPS formation) (see Fig. 3). Thus, sludge settleability decreased in both systems with DSVI finally increasing to almost 900 cm^3/g and 2300 cm^3/g for *Viscous* and *Filamentous system*, respectively (see Fig. 4).

As shown in Fig. 4, viscous bulking caused a continuous increase in DSVI in *Viscous system* from Day 6 of operation until the end of the experiment. In contrast, the abundance of filaments did not change significantly in the first 2 weeks in *Filamentous system*, however, a sharp increase in DSVI can be seen from Days 13–14. Due to the poor sludge settleability, the secondary clarifiers were filled up with bulking sludge all along the experiment in both systems, finally, resulting in sludge overflow on Day 30 (see photos in Fig. 3): COD concentration peak values of 4050 $mgCOD/l$ and 323 $mgCOD/l$ were measured in *Viscous system* and *Filamentous system*, respectively (Figure A.1 in Appendix A. Supplementary Information). This led also to the undesired dilution of bioreactor mixed liquor in *Viscous system* resulting in a decrease of MLSS to 2.8 g/l in the last week of the experiment. MLSS concentration was continuously decreasing in *Filamentous system* due to the very low growth rate of microorganisms under the applied low S - low DO conditions and to the inevitable daily sampling of ca. 0.5 l mixed liquor for analysis.

The initial EPS content of 7w/w% started to increase on Day 10 (17 w/w%) and achieved 42 w/w% at the end of the experiment in *Viscous system*. In the case of *Filamentous system* the filament abundance started to increase around Days 13–14, reached a value of 60% within 5 days and finally 87% (expressed in covered microscopic picture area %) at the end of the experiment (see Fig. 4 c) and d)). Microscopical observations of native and stained sludge samples (see Fig. 3) showed that the initial well-settling (reference) sludge contained a low quantity of *Microthrix parvicella* and few *Nostocoida limicola II, Type 021N* and *Type 0041* species. The serious bulking was generated primarily through the overgrowth of *Nostocoida limicola II* (coupled with *Nostocoida limicola I* and *III* species as well), *Thiothrix* and *Sphaerotilus natans* followed by the presence of some *Microthrix parvicella, Type 021N* and *Type 0041*. As illustrated in Fig. 4 b) and d) the DSVI showed strong correlation with the EPS content in *Viscous system* and also with the filament abundance in *Filamentous system* with Spearman correlation coefficients of $RSP_{System1}(EPS-content; DSVI) = 1$ and $RSP_{System2}(Filament - content; DSVI) = 0.932$, respectively. These results for *Viscous system* are in good concordance with the relationship between EPS content and SVI published by Jobbágy et al. (2002).

At the start of the experiment, after some days of adaptation the COD removal efficiency of *Viscous system* exceeded 90% (Figure A.1 a) in Appendix A. Supplementary Information). Then after one week effluent COD started to increase in a monotonic manner then this change accelerated and finally jumped to as high as 4000 mg/l due to (i) deteriorated sludge settleability and (ii) limited oxygen and soluble substrate transfer caused by overproduction of EPS (COD removal decreased from $>$ 95% to approx. 75%). In *Filamentous system* the COD removal efficiency was around 85% all along the experiment except for the final date (Figure A.1 b) in Appendix A. Supplementary Information) when sludge overflow occurred in both systems from the fully filled secondary clarifiers resulting in effluent COD (and TSS) concentration peaks.

The capillary suction time (CST) of the initial reference (ideal-like) sludge was low (6.7 s). In the *Filamentous system* CST remained almost constant (varied in the range of 5.7 - 6.7 s) during the whole experiment.

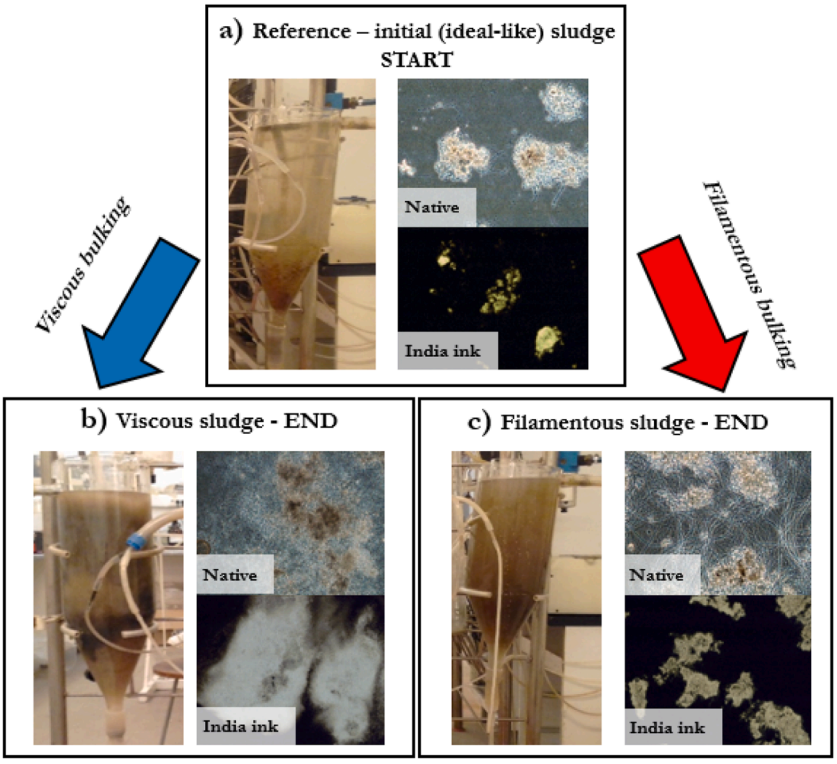

Fig. 3. Photographs of secondary clarifiers and pictures of AS microscopic observations (Native in phase contrast, magn. 200x and India ink staining, magn. 100x): a) Reference (initial ideal-like) sludge at the start in both experimental systems, b) Viscous sludge and c) Filamentous sludge at the end of the experiment.

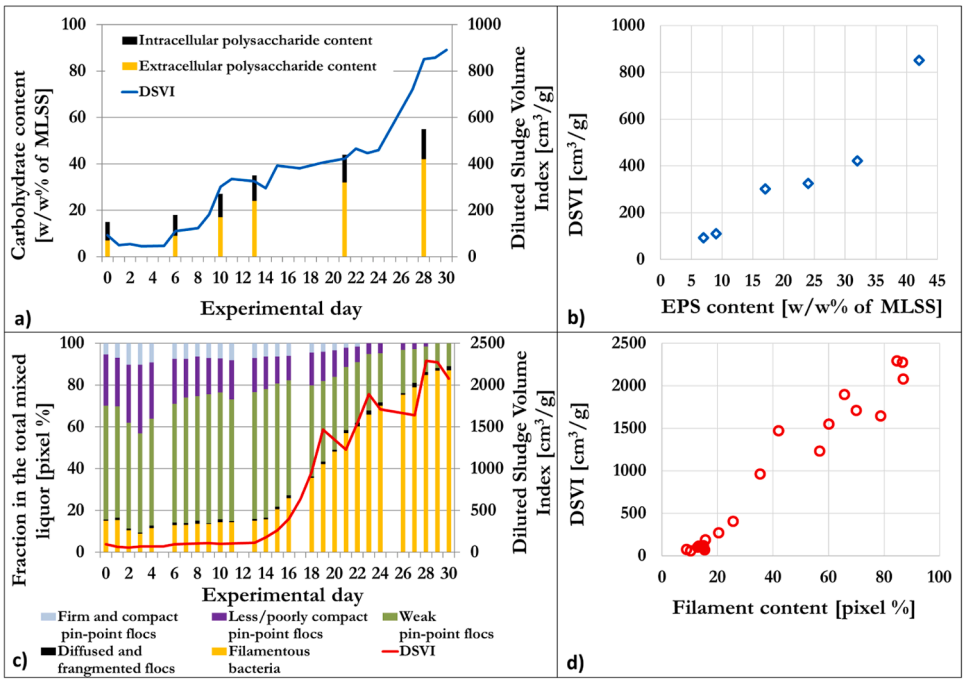

Fig. 4. Changes in a) DSVI and EPS content in *Viscous system* and b) relation between DSVI and EPS content as well as changes in c) DSVI and filamentous bacteria abundance in *Filamentous system* and d) relation between DSVI and filament content during the experiment.

However, viscous bulking led to high CST values reaching 250 *s* already on Day 10 and increased continuously, leading to an extremely poorly filterable sludge with a CST of 573 *s* on Day 28. The high CST values were coherent with the poor sludge filterability all along the experiment in *Viscous system*.

3.2. Results of rheological investigations and the parameter set measured

The viscosity curves of both *Viscous* and *Filamentous system* measured at the end of the experiment, as well as referring data of the initial reference sludge showed a pronounced shear-thinning behavior, as expected from semi-concentrated sludge suspensions (Fig. 5).

We observed a striking difference between the rheological properties of the two systems at the end of the experiment. The viscosity values of *Filamentous system* changed to a smaller extent than in the case of the viscous sludge compared to the initial (reference) sludge which can be explained by the softness and higher deformability of the filaments, seemingly unable to form a stiff network structure and, consequently, easy to be broken down by shear stress. Contrarily, the *Viscous system* exhibited large viscosity values even at high shear rates due to (i) the increase of the viscosity of the suspending liquid (caused by EPS); (ii) the embedment of the AS flocs in the gelled bulk medium. The slope of the curves is similar, apparently, they seemingly differ by a constant multiplier only. Data points of the viscosity curves were fit to Power-law (PL), Bingham (B) and Herschel-Bulkley (HB) rheological models. HB has been proved to be the most accurate indicated by the high coefficients of determination of the fit for both systems (Table 3).

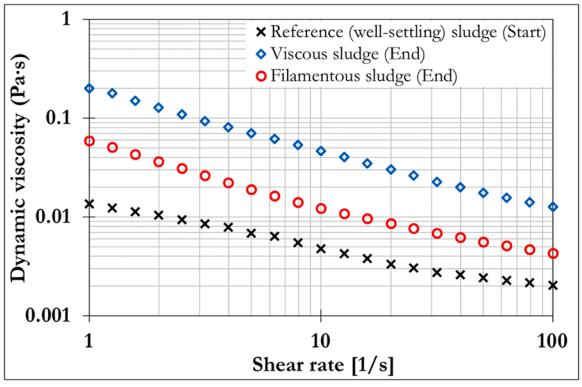

Fig. 5. Dynamic viscosity values measured for the Reference (ideal-like) sludge at the start; for the *Viscous* and *Filamentous system* at the end of the experiment.

PL ignores the existence of yield stress which appears at the final stage of the *Viscous system*, while the B model does not describe the non-linearity of the rheological behavior of the sludge resulting in a less accurate fit as compared to the HB model. Therefore, the changes of rheological parameters over time are shown only for the HB model in Fig. 6 a-c), while those for PL and B models can be found in Appendix A. Supplementary Information (Figures A.2–3). Both systems preserved their shear-dependent behavior for the whole time range of the experiment (Fig. 6 a)), also supported by PL (as shown in Figure A.2). Remarkable changes in all of the HB fluid properties could be observed only after Day 20 for *Viscous system* (Fig. 6). The least significant change

Table 3
Rheological parameters of the material models (Power-law: PL, Bingham: B; Herschel-Bulkley: HB) used in CFD simulations with the related coefficients of determination of the fit.

Parameter [unit]	Reference (well settling) sludge (Start)	Viscous sludge (End)	Filamentous sludge (End)
PL - k [$Pa{\cdot}s^n$]	0.0104	0.1669	0.0405
PL - n [-]	0.6361	0.4255	0.4987
PL - R^2 [-]	0.9923	0.9943	0.9883
B - $\tau_{0,B}$ [Pa]	0.0224	0.2858	0.0769
B - μ_B [$Pa{\cdot}s$]	0.0019	0.0105	0.0037
B - R^2 [-]	0.9881	0.9524	0.9796
HB - $\tau_{0,HB}$ [Pa]	0.0122	0.1108	0.0452
HB - μ_{HB} [$Pa{\cdot}s^n$]	0.0053	0.0922	0.0157
HB - n_{HB} [-]	0.7743	0.5389	0.6900
HB - R^2 [-]	0.9977	0.9985	0.9998

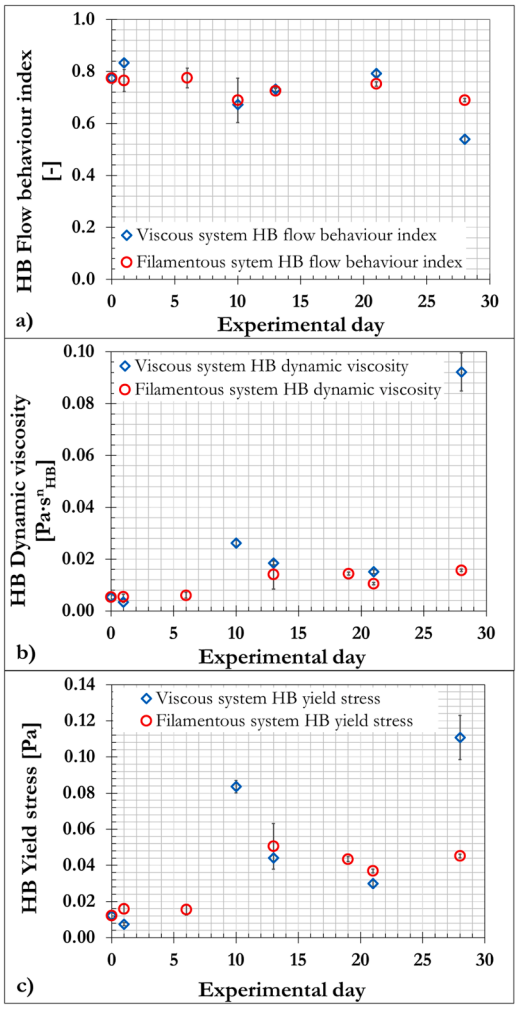

Fig. 6. The fit of rheological parameters to the measured data by the Herschel-Bulkley model: a) flow behaviour index; b) dynamic viscosity; c) yield stress.

was in the flow behavior index, which was nearly constant during the experiment in both cases (Fig. 6 a)). The HB Dynamic viscosity and HB Yield stress increased steadily and slowly during the study for *Filamentous system* (Fig. 6 b) and c)). In the latter case, the small increase of yield stress (compared to *Viscous system*) indicated the absence of a stiff structure and the formation of only a very loose connection between solid parts (confirmed also by yield stress calculated from the B model as shown in Figure A.3).

Viscosity and flow properties have been proved to be dependent on sludge floc structure. B and HB yield stresses, B and HB dynamic viscosities showed a linear correlation with the indicators of biomass structures (i.e. EPS or filament content) and with the DSVI (Table 4). Fig. 7 shows the relationship between the floc structure and the two parameters of the HB model for both systems. It should be emphasized that the dynamic viscosity changed significantly in *Viscous system* and *Filamentous system* as well.

3.3. Results of computational fluid dynamics studies

In industrial applications, sludge is transported through pipelines and pipe fittings typically at a mean velocity of $0.5 - 2m/s$ KSB (2005); Rötsch (1999). For the present fluids, this represents turbulent flow conditions in the Reynolds number range of $Re_{mod} = 2200 - 100000$. Although our calculations were performed for only one geometry, results obtained for the friction and loss coefficients may be widely applicable due to the generalization of the Reynolds number.

Table 4
Correlation coefficients between the measured rheological and structural parameters (EPS and filament content) and settleability (DSVI) for the two different biomass structures generated.

	Viscous system		*Filamentous system*	
Parameter	DSVI	EPS content	DSVI	Filament content
PL - k	0.67	0.57	0.61	0.56
PL - n	–0.27	0.1	–0.47	–0.46
B - $\tau_{0.B}$	0.71	0.67	0.67	0.61
B - μ_B	0.93	0.78	0.78	0.70
HB - $\tau_{0.HB}$	0.74	0.5	0.61	0.57
HB - μ_{HB}	0.71	0.67	0.74	0.67
HB - n_{HB}	–0.68	–0.45	–0.55	–0.52

The predicted friction factors are presented as a function of the Re_{mod} (Fig. 8a) diagram). The average difference between our calculated friction factors and the $f = 64/Re_{mod}$ curve was 5% (and similarly in the turbulent region as well).

Fig. 8b) shows the dimensionless loss coefficient (ζ) of the elbow calculated for the three different biomass structures (i.e. blue: reference (ideal-like); red: viscous; black: filamentous), with the three models applied (i.e. PL, H and HB). For turbulent flows (typical for full-scale applications) the coefficients calculated for the same biomass structure (i.e. same colour) seem to be arranged along straight lines in the log-log scale diagram.

For appropriate sizing of hydraulic systems in WWTPs, the pressure drop caused by pipe elements has to be estimated at different flow velocities (Fig. 9). In our work the pressure losses of the elbow were also determined for clean water, commonly used as a reference in design practice. On one hand, in the highlighted flow velocity range of $v = 0.5 - 2m/s$ the pressure losses of the reference (well settling) sludge were 33% higher than those of the clean water on average (considered for all flow velocities and models). The highest increase in pressure drop was gained by the B fluid model for viscous sludge at $v = 0.5m/s$ compared to the clean water, i.e. the value calculated for water increased by 170% (see the small column chart in Fig. 9). This increase was 135% by HB model. On the other hand, as for comparing viscous and filamentous sludge to the initial reference (ideal-like) sludge by HB model in the range of $v = 0.5 - 2m/s$, the pressure loss increased by 59% in the *Viscous system*, while this increase in the *Filamentous system* was 22% on average. The relative difference between the estimated pressure drops decreased with the increase of the mean velocity. In the case of *Filamentous system* the standard deviation of the pressure drop values calculated by the different rheological models was within 10%, thus in this system the applied rheological model had no significant effect. Model selection becomes more important with the increase of viscosity and/or the decrease of flow velocity.

3.4. Relationship between structural changes and hydrodynamic behavior

Based on the rheological fit and the hydrodynamic simulations, the Re_{mod} dependent loss coefficients of the examined elbow could be estimated for the entire period of the experiment (from "Start" to "End"). For this evaluation the HB model was applied in the Re_{mod} range of $5000 - 110000$. The estimated relationship for the loss coefficient was: $\zeta_{HB} = 4.9539 * Re_{mod}^{-0.282}$ (Figure A.4 in Appendix A. Supplementary Information).

The calculated pressure drop on the elbow is shown in Fig. 10 at $v = 1m/s$ average flow velocity as a function of EPS content and filamentous bacteria abundance in *Viscous system* and *Filamentous system*, respectively. The pressure losses on the elbow have been proved to be closely related to the changes of floc micro-structure in the case of viscous bulking (*Viscous system*). The correlation coefficient between the

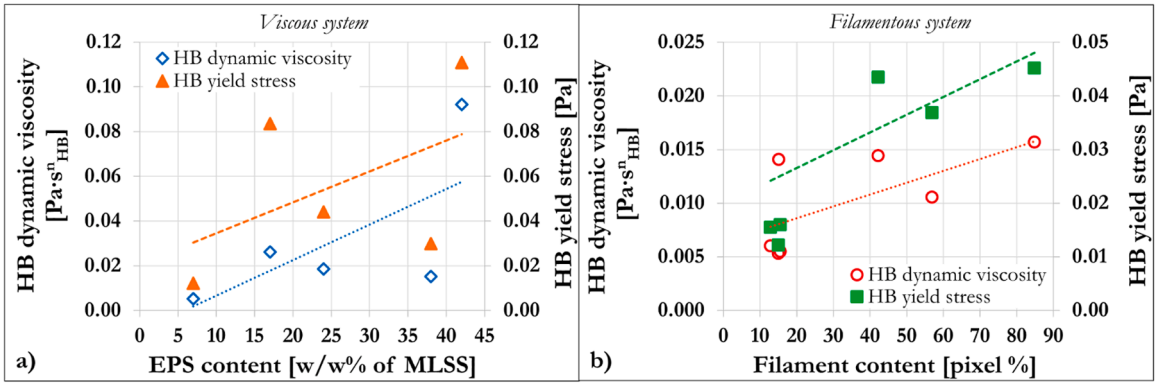

Fig. 7. Relationship between the AS floc structure characterizing indicators (EPS and filament content), the HB dynamic viscosity and the yield stress in a) *Viscous system*; b) *Filamentous system*.

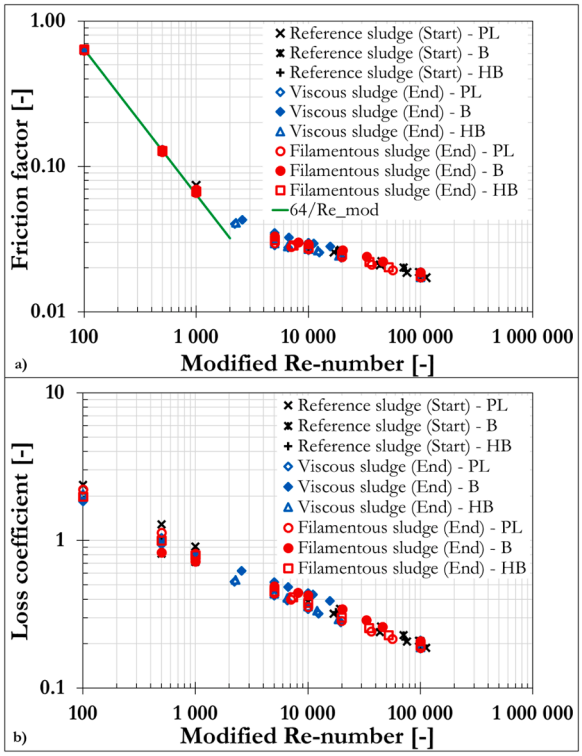

Fig. 8. a) Calculated and analytical ($64/Re_{mod}$) friction factor of straight pipe and b) calculated loss coefficients of an elbow with the relative radius of curvature of $r/D = 1$ as a function of the modified Reynolds-number.

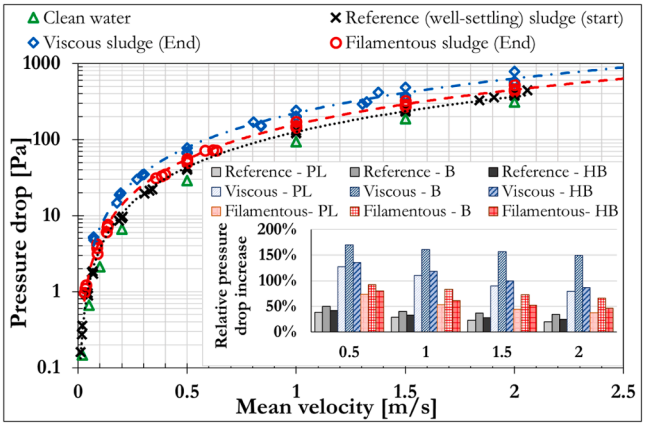

Fig. 9. Pressure drop on the elbow as a function of the average flow velocity. In addition the relative pressure drop increase compared to clean water at flow velocities of $0.5; 1; 1.5; 2 m/s$ (small column chart).

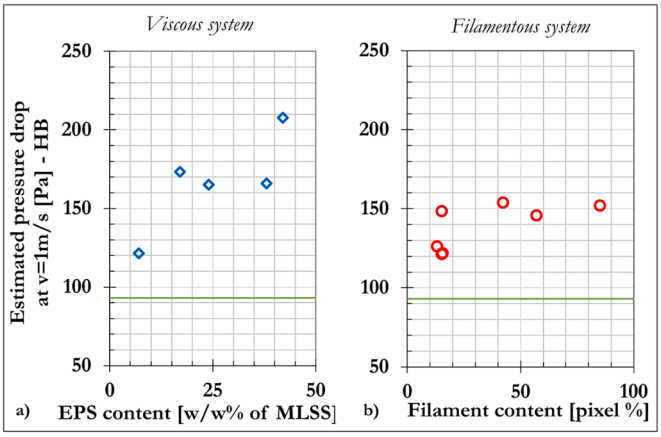

Fig. 10. Estimated pressure drop on the elbow calculated at $v = 1 m/s$ by Herschel-Bulkley model as a function of a) the EPS content for *Viscous system*, $R = 0.81$; b) the filament content for *Filamentous system*, $R = 0.68$. Solid line: pressure drop in case of clean water.

pressure drop and the EPS content was $R = 0.81$. In *Filamentous system* an increase of the pressure drop could definitely be observed with the growing ratio of filaments, however, correlation coefficient showed a loose relationship ($R = 0.68$).

4. Outlook and perspectives

The advanced standard protocol, developed for modelling both viscous and filamentous bulking by rheological approach, may serve as useful tool for improving energy efficiency of sludge pumping at municipal and/or industrial AS WWTPs facing high energy consumption as well as seasonal or permanent sludge separability issues. Estimations calculated for pressure loss in pipe elements may be taken into consideration in state-of-the-art design protocols of hydraulic systems (i.e. sizing of pipes and fittings, pump selection). Although calculations were carried out for an MLSS concentration typically applied in conventional AS bioreactors, the new concept and the results may be applicable and adaptable in a wide range of the given dimensionless parameters (e.g. for sludge flows in sludge treatment and dewatering processes).

5. Conclusions

Severe viscous and filamentous kinds of bulking were successfully generated under controlled experimental conditions in two separate continuous-flow lab-scale systems seeded with the same well settling (ideal-like) reference sludge at the start. Results suggest correlation between DSVI and EPS content in *Viscous system* and, similarly, between DSVI and filamentous bacteria abundance in *Filamentous system*.

- Both viscous and filamentous floc structures showed strongly non-Newtonian behavior during the whole experiment indicated by consistency index values significantly lower than 1. Viscosity and yield stress values determined from rheological models showed distinct tendencies for the two systems. Although we obtained some correlation between the change of floc structure and rheological properties in both cases, viscous bulking had a more pronounced effect on the flow behavior than filamentous bulking.
- Model discrimination showed that the Herschel-Bulkley model has the best fit (vs. Power-law and Bingham) for describing flow properties of the investigated floc structures. Thus, rheology has been proved to be a useful complementary tool for the quick identification of dominant bulking mechanism.
- The CFD studies determined the effect of AS floc structure changes on the friction factor, the loss coefficient and the pressure drop of a typical pipe elbow configuration investigated. The pressure loss was significantly higher in the case of non-Newtonian flows compared to the clean water and viscous bulking generated the largest pressure loss values. The increase of the pressure losses calculated for viscous and filamentous biomass was also remarkable compared to the reference (ideal-like) sludge.
- A standard protocol has been developed for hydrodynamic modelling of both viscous and filamentous bulking which has been proved to be efficient for analyzing the energy consumption of nitrate recirculating and sludge recirculating pumps at WWTPs and calculating pressure loss for different sludge floc structures.
- To our knowledge this has been the first time when the entire evolution of both viscous and filamentous bulking was comprehensively analyzed and tracked by detailed biochemical and rheological measurements at a fixed biomass concentration (3.5 $g\ /l$), as well as combined by further hydrodynamic modelling. Research results provided a powerful tool for improving energy efficiency of sludge pumping.

Declaration of Competing Interest

The authors declare that they have no known competing financial interests or personal relationships that could have appeared to influence the work reported in this paper.

Acknowledgment

The cross-border cooperation was supported both by Hungarian National Research, Development and Innovation Office (TÉT-14-FR-1-2015-0033) and Campus France (PHC Balaton No.34474QA). Professional contribution of Michele Delalonde and the technical help of Emilie Ruiz (UMR QualiSud, University of Montpellier) is highly acknowledged. Additional support of the Higher Education Excellence Program of the Ministry of Human Capacities (EMMI) within the frame of both Biotechnology and Water Science and Disaster Prevention research areas of Budapest University of Technology and Economics (BME FIKP-BIO and FIKP-VIZ) is also highly appreciated. Authors acknowledge the János Bolyai Research Scholarship of the Hungarian Academy of Sciences and the ÚNKP-19-4-BME-421, ÚNKP-20-5-BME-156, ÚNKP-21-5-BME New National Excellence Program of the Ministry of Human Capacities.

Supplementary material

Supplementary material associated with this article can be found, in the online version, at Doi:10.1016/j.watres.2022.118155

References

ANSYS, I., 2011. ANSYS CFX-Solver Theory Guide. Southpointe 275 Technology Drive Canonsburg, PA 1531.URL:http://www.ansys.com

APHA, 1999. Standard Methods for the Examination of Water and Wastewater, 20th. AMERICAN PUBLIC HEALTH ASSOCIATION, Washington DC, US.

Bakos, V., Deák, A., Jobbágy, A., 2019. Reconsideration and upgrading of sampling and analysis methods for avoiding measurement-related design and operation failures in wastewater treatment. Water SA 45 (3), 329–337. https://doi.org/10.17159/wsa/2019.v45.i3.6729.

Bakos, V., Kiss, B., Jobbágy, A., 2016. Problems and causes of marginal nutrient availability in winery wastewater treatment. Acta Alimentaria Hungarica 45 (4), 532–541. https://doi.org/10.1556/066.2016.45.4.10.

Baroutian, S., Eshtiaghi, N., Gapes, D.J., 2013. Rheology of a primary and secondary sewage sludge mixture: dependency on temperature and solid concentration. Bioresour. Technol. 140, 227–233. https://doi.org/10.1016/j.biortech.2013.04.114.

Baudez, J., 2008. Physical aging and thixotropy in sludge rheology. Applied Rheology 18 (1), 13495-1–13495-8. https://doi.org/10.1515/arh-2008-0003.

Baudez, J.C., Gupta, R.K., Eshtiaghi, N., Slatter, P., 2013. The viscoelastic behaviour of raw and anaerobic digested sludge: strong similarities with soft-glassy materials. Water Res. 47, 173–180. https://doi.org/10.1016/j.watres.2012.09.048.

Cabral, R.A., Telis, V.R., Park, K.J., Telis-Romero, J., 2011. Friction losses in valves and fittings for liquid food products. Food Bioprod. Process. https://doi.org/10.1016/j.fbp.2010.08.002.

Csizmadia, P., Hos, C., 2014. CFD-based estimation and experiments on the loss coefficient for bingham and power-law fluids through diffusers and elbows. Computers and Fluids 99, 116–123. https://doi.org/10.1016/j.compfluid.2014.04.004.

Csizmadia, P., Till, S., 2018. The effect of rheology model of an activated sludge on to the predicted losses by an elbow. Periodica Polytechnica Mechanical Engineering 62, 305–311. https://doi.org/10.3311/PPme.12348.

Eshtiaghi, N., Markis, F., Yap, S.D., Baudez, J.C., Slatter, P., 2013. Rheological characterisation of municipal sludge: areview. Water Res. 47, 5493–5510. https://doi.org/10.1016/j.watres.2013.07.001.

Eshtiaghi, N., Yap, S., Markis, F., Baudez, J., Slatter, P., 2012. Clear model fluids to emulate the rheological properties of thickened digested sludge. Water Res. 46, 3014–3022. https://doi.org/10.1016/j.watres.2012.03.003.

Farno, E., Baudez, J., Parthasarathy, R., Eshtiaghi, N., 2016. The viscoelastic characterisation of thermally-treated waste activated sludge. Chemical Engineering Journal 304, 362–368. https://doi.org/10.1016/j.cej.2016.06.082.

Filali, A., Khezzar, L., Mitsoulis, E., 2013. Some experiences with the numerical simulation of newtonian and bingham fluids in dip coating. Computers and Fluids 82, 110–121. https://doi.org/10.1016/j.compfluid.2013.04.024.

Hii, K., Farno, E., Baroutian, S., Parthasarathy, R., Eshtiaghi, N., 2019. Rheological characterization of thermal hydrolysed waste activated sludge. Water Res. 156, 445–455. https://doi.org/10.1016/j.watres.2019.03.039.

Hii, K., Parthasarathy, R., Baroutian, S., Gapes, D., Eshtiaghi, N., 2017. Rheological measurements as a tool for monitoring the performance of high pressure and high temperature treatment of sewage sludge. Water Res. 114, 254–263. https://doi.org/10.1016/j.watres.2017.02.031.

Hong, E., Yeneneh, A.M., Kayaalp, A., Sen, T.K., Ang, H.M., Kayaalp, M., 2016. Rheological characteristics of municipal thickened excess activated sludge (teas): impacts of ph, temperature, solid concentration and polymer dose. Res. Chem. Intermed. 42 (8), 6567–6585. https://doi.org/10.1007/s11164-016-2482-22.

Hong, E., Yeneneh, A.M., Sen, T.K., Ang, H.M., Kayaalp, A., 2018. A comprehensive review on rheological studies of sludge from various sections of municipal wastewater treatment plants for enhancement of process performance. Adv Colloid Interface Sci 257, 19–30. https://doi.org/10.1016/j.cis.2018.06.002.

Jenkins, D., Richard, M., Daigger, G., 2004. Manual on the causes and control of activated sludge bulking, foaming, and other solids separation problems, 3rd. CRC Press LLC, Florida, US.

Jobbágy, A., Kiss, B., Bakos, V., 2017. Conditions favoring proliferation of glycogen accumulating organisms for excess biological carbon removal in treating nutrient deficient wastewater. Periodica Polytechnica Chemical Engineering 61, 149–155. https://doi.org/10.3311/PPch.10078.

Jobbágy, A., Literáthy, B., Tardy, G., 2002. Implementation of glycogen accumulating bacteria in treating nutrient-deficient wastewater. Water Sci. Technol. 46 (1), 185–190. https://doi.org/10.2166/wst.2002.0475.

Jobbágy, A., Németh, N., Altermatt, R., Samhaber, W., 2000. Encouraging filament growth in an activated sludge treatment plant of the chemical industry. Water Res. 34 (2), 699–703. https://doi.org/10.1016/S0043-1354(99)00149-9.

Jobbágy, A., Weinpel, T., Bakos, V., Vánkos, Z., 2019. Use of floating seals to exclude oxygen penetration in non-aerated selectors. Water Sci. Technol. 80 (2), 357–364. https://doi.org/10.2166/wst.2019.280.

Kfuri, S., Silva, J., Soares, E., Thompson, R., 2011. Friction losses for power-law and viscoplastic materials in an entrance of a tube and an abrupt contraction. Journal of Petroleum Science and Engineering 76, 224–235. https://doi.org/10.1016/j.petrol.2011.01.002.

Khandelwal, V., Dhiman, A., Baranyi, L., 2015. Laminar flow of non-newtonian shear-thinning fluids in a t-channel. Computers and Fluids 108, 79–91. https://doi.org/10.1016/j.compfluid.2014.11.030.

Kiss, B., Bakos, V., Liu, W.T., Jobbagy, A., 2011. Full-scale use of glycogen-accumulating organisms for excess biological carbon removal. Water Environ. Res. 83, 855–864. https://doi.org/10.2175/106143010X12851009156844.

KSB, 2005. Selecting centrifugal pumps, 4th. KSB Aktiengesellschaft Communications, Frankenthal, Germany.

Liu, M., Duan, Y.F., 2009. Resistance properties of coal-water slurry flowing through local piping fittings. Exp. Therm Fluid Sci. 33 (5), 828–837. https://doi.org/10.1016/j.expthermflusci.2009.02.011.

Madlener, K., Frey, B., Ciezki, H.K., 2009. Generalized reynolds number for non-newtonian fluids. Progress in Propulsion Physics 1, 237–250. https://doi.org/10.1051/eucass/200901237.

Metzner, A., Reed, J., 1955. Flow of non-newtonian fluids-correlation of the laminar, transition, and turbulent-flow regions. AlChE J. 1, 434–440. https://doi.org/10.1002/aic.690010409.

Monteiro, A.C., Bansal, P.K., 2010. Pressure drop characteristics and rheological modeling of ice slurry flow in pipes. Int. J. Refrig 33, 1523–1532. https://doi.org/10.1016/j.ijrefrig.2010.09.009.

Mori, M., Seyssiecq, I., Roche, N., 2006. Rheological measurements of sewage sludge for various solids concentrations and geometry. Process Biochem. 41, 1656–1662. https://doi.org/10.1016/j.procbio.2006.03.021.

Motta, M., Pons, M.N., Roche, N., Vivier, H., 2001. Characterisation of activated sludge by automated image analysis. Biochem. Eng. J. 9, 165–173. https://doi.org/10.1016/S1369-703X(01)00138-3.

Nagy Göde, P., 2010. Characterization of activated sludge floc structure by optical software analysis. Vízmű Panoráma 18 (8), 22–23(in Hungarian).

Pinho, F.T., Whitelaw, J.H., 1990. Flow of non-newtonian fluids in a pipe. Journal of Non-Newtonian Fluid Mechanics Elsevier Science Publishers B.V 34, 129–144.

Ratkovich, N., Horn, W., Helmus, F.P., Rosenberger, S., Naessens, W., Nopens, I., Bentzen, T.R., 2013. Activated sludge rheology: a critical review on data collection and modelling. Water Res. 47, 463–482. https://doi.org/10.1016/j.watres.2012.11.021.

Rötsch, D., 1999. Zuverlässigkeit von Rohrleitungssystemen, 1st. Springer, Berlin, Heidelberg. https://doi.org/10.1007/978-3-642-60217-7.

Seyssiecq, I., Ferrasse, J.H., Roche, N., 2003. State-of-the-art: rheological characterisation of wastewater treatment sludge. Biochem. Eng. J. 16, 41–56. https://doi.org/10.1016/S1369-703X(03)00021-4.

Seyssiecq, I., Marrot, B., Djerroud, D., Roche, N., 2008. In situ triphasic rheological characterisation of activated sludge, in an aerated bioreactor. Chemical Engineering Journal 142, 40–47. https://doi.org/10.1016/j.cej.2007.11.007.

Singh, R.K., Singh, S.N., Seshadri, V., 2010. CFD prediction of the effects of the upstream elbow fittings on the performance of cone flowmeters. Flow Meas. Instrum. 21, 88–97. https://doi.org/10.1016/j.flowmeasinst.2010.01.003.

Stickland, A., 2015. Compressional rheology: a tool for understanding compressibility effects in sludge dewatering. Water Res. 82, 37–46. https://doi.org/10.1016/j.watres.2015.04.004.

Swamee, P.K., Aggarwal, N., 2011. Explicit equations for laminar flow of bingham plastic fluids. Journal of Petroleum Science and Engineering 76, 178–184. https://doi.org/10.1016/j.petrol.2011.01.015.

Swamee, P.K., Aggarwal, N., 2011. Explicit equations for laminar flow of herschel-bulkley fluids. Can. J. Chem. Eng. 89, 1426–1433. https://doi.org/10.1002/cjce.20484.

Tardy, G.M., Bakos, V., Jobbágy, A., 2012. Conditions and technologies of biological wastewater treatment in hungary. Water Sci. Technol. 65 (9), 1676–1683. https://doi.org/10.2166/wst.2012.062.

Vachoud, L., Ruiz, E., Delalonde, M., Wisniewski, C., 2019. How the nature of the compounds present in solid and liquid compartments of activated sludge impact its rheological characteristics. Environ Technol 40 (1), 60–71. https://doi.org/10.1080/09593330.2017.1378729.

Wágner, D., Ramin, E., Szabo, P., Dechesne, A., Plósz, B.G., 2015. *Microthrix parvicella* abundance associates with activated sludge settling velocity and rheology - quantifying and modelling filamentous bulking. Water Res. 78, 121–132. https://doi.org/10.1016/j.watres.2015.04.003.

Wang, H.F., Ma, Y.J., Wang, H.J., Hu, H., Yang, H.Y., Zeng, R., 2017. Applying rheological analysis to better understand the mechanism of acid conditioning on activated sludge dewatering. Water Res. 122, 398–406. https://doi.org/10.1016/j.watres.2017.05.002.

Wanner, J., Jobbágy, A., 2014. Activated sludge solids separations. Activated Sludge - 100 Years and Counting. IWA Publishing, Glasgow, UK, pp. 171–194.

White, F.M., 1991. Viscous Fluid Flow, 2nd. McGraw-Hill, Inc., New York, USA.

Zhang, Z., Zeng, Y., Kusiak, A., 2012. Minimizing pump energy in a wastewater processing plant. Energy 47, 505–514. https://doi.org/10.1016/j.energy.2012.08.048.